



# A Numerical Investigation on the Combined Effect of Aluminum-Nitride/Water Nanofluid with Different Mini-Scale Geometries for Passive Hydrothermal Augmentation

Open  
Access

Nura Muaz Muhammad<sup>1,3\*</sup>, Nor Azwadi Che Sidik<sup>1,2</sup>, Aminuddin Saat<sup>1</sup>, Yusuf Alhassan<sup>3</sup>, Yutaka Asako<sup>2</sup>

<sup>1</sup> School of Mechanical Engineering, Universiti Teknologi Malaysia, 81310 Skudai, Johor, Malaysia

<sup>2</sup> Malaysia-Japan International Institute of Technology (MJIT), Universiti Teknologi Malaysia, Jalan Sultan Yahya Petra, Kuala Lumpur, Malaysia

<sup>3</sup> Faculty of Engineering, Kano University of Science and Technology, Wudil, PMB 3244, Kano, Nigeria

## ARTICLE INFO

### Article history:

Received 23 April 2020

Received in revised form 15 June 2020

Accepted 22 June 2020

Available online 30 June 2020

## ABSTRACT

Variation of channel geometry can be regarded as one of the passive heat transfer enhancement techniques in thermal devices. Comparison of different geometries under similar condition can offer more insight into their capabilities in thermal design and management. This investigation involves convective single-phase heat transfer and flow of a 3D computational domain filled with AlN-water nanofluid. The bottom wall subjected to a constant heat flux of  $85 \text{ W/cm}^2$ , while the top wall is lagged, and the sides walls are considered both as symmetry and adiabatic. The dimensionless parameters used include Reynolds number ( $5000 \leq Re \leq 10000$ ) and nanoparticle volume fractions ( $\phi = 0.00, 0.01$  and  $0.03$ ). The hydraulic diameter  $D_h = 1.111 \text{ mm}$  adopted for ease of comparison as the common dimension for all the geometries namely: square, wavy and rectangular minichannels. The results correlate reasonably well when compared with similar experimental results in the literature. It was found that the highest temperature for the fluid-solid boundary of the minichannels was  $328 \text{ K}$  at  $Re 5000$  for the square channel which is below the desired upper limit of  $353 \text{ K}$  for the enclosed electronic devices. The results affirmed that nanofluid induction into the minichannels assists in the improvement of heat transfer which increases with the addition of volume fraction of the nanoparticle and Reynolds number. The wavy minichannel has better hydrothermal performance than the straight minichannels.

### Keywords:

Minichannel; volume fraction; Turbulent flow; Pressure drop; Hydrothermal; Passive augmentation

Copyright © 2020 PENERBIT AKADEMIA BARU - All rights reserved

## 1. Introduction

Research and development of devices and system are taking a new paradigm due to recent technological advancement, which requires highly efficient and compact devices and systems. But with a penalty on high heat flux generation which must be evacuated instantly and promptly to safeguard the devices and system from untimely failure. Researchers employ different passive heat

\* Corresponding author.

E-mail address: [nuramuaz@gmail.com](mailto:nuramuaz@gmail.com) (Nura Muaz Muhammad)

transfer mechanism to achieve this task like modifying the flow cavity as well as the use of working fluid with high thermal conductivity. Choi *et al.*, [1] observed that addition of nanometer-sized solid of either metallic, ceramics or carbon allotropes into the conventional fluids like water and oil can enhance their thermal conductivity and eventually improves their heat transfer performance. Many researchers employed various types of these innovative fluids named as Nanofluids with good results. [2]–[4]

Aluminum-Nitride (AlN) as non-oxide ceramic solid phase has been recognised and used as an additive in heat transfer nanofluid as a result of its high thermal conductivity by few researchers [5]–[7]. Baker *et al.*, [8] synthesis AlN nanoparticles by a Reactive Gas Condensation (RGC) with an Ammonia as the reactive gas and a Nitrogen both as a carrier and inert source gas for the nitridation of Aluminum. Also, Zhao and Gao [9] prepared AlN with thermal conductivity as high as 264.5 W/mK by gas sintering with  $Y_2O_3$  nanoparticle concentration of 2 – 4% as sintering aids.

Researchers observed that the thermophysical properties of a nanofluid to be used as a thermal transport fluid must be assessed and certified to have optimal efficiency. Taha *et al.*, [10] investigated the thermophysical properties particularly, thermal conductivity and viscosity and morphological attributes of the dielectric insulating oil-based homogenous nanofluid containing AlN and TiO nanoparticles. They reported their stability enhanced whilst maintaining thermal properties. Yu *et al.*, [11] observed minimal effect of temperature on the thermal conductivity ratios of colloids containing AlN nanoparticles with a volume fraction of 0.1 in Ethylene (ETG) and Propylene glycols (PPG) liquids, though with an improvement of 38.7 % and 40.2%, correspondingly for ETG and PPG.

Zyla and Fal [12] experimented on physical properties of AlN-ETG nanofluid produced by the two-step method. At a uniform temperature of 298.15K, they measured dynamic viscosity with shear rates between  $1e^{-2}$  and  $1000s^{-1}$  at 0.1MPa pressure. They reported that AlN-ETG nanofluid show non-Newtonian behaviour where the thermal conductivity increases linearly with the nanoparticle's concentration. However, Wozniak *et al.*, [13] investigated the applicability of AlN-PPG as the thermal liquid in a closed system due to its remarkable heat conductivity as high as 320 W/m.K and found that the nanofluid exhibits a Newtonian behaviour at increasing temperature and shear rate, and high flowability with prolonged stability.

From the available literature reviewed and presented above, a study of AlN nanoparticle as a solid phase in thermal transmission nanofluids with water as a base fluid has not been embarked, despite its abundance and high solvent ability. Thus, this study intends to exploit passive heat transfer technique of a thermal and transport medium in cooling of electronic devices by combining AlN-DI Water nanofluid with the solid mediums in minichannel range to certify the geometry with optimum hydrothermal thermal performance.

## 2. Numerical Formulation

### 2.1 Model Geometry and Boundary Conditions

The analysis involves the study of the time-dependent forced convection heat transfer and flows in three different geometries, namely: square, wavy and rectangular minichannels to save the volume of fluid due to their high surface area to volume ratio. The computational domain has dimensions (in mm for x,y,z) 2.5, 2.25 and 30, respectively, while the hydraulic diameter is 1.111mm for uniformity. The geometrical details of the minichannels are expressed in Table 1.

**Table 1**  
 Geometrical values of the minichannels

Case No	Designation	Name	Wc	Hc
1	C1	Square	1.111	1.111
2	C2	Wavy	1.000	1.250
3	C3	Rectangular	1.000	1.250

## 2.2 Thermophysical Properties of the Fluids

In this work, the nanofluid contains Aluminum-Nitride nanoparticles of size 40nm and volume fractions of 0.01 and 0.03 dispersed into pure water as base fluid. Their thermophysical properties were mentioned in Table 2.

**Table 2**  
 Thermophysical properties of different materials at 303.15K [14]

Properties	Density (kg/m <sup>3</sup> )	Specific heat (J/kgK)	Thermal conductivity (W/mK)	Dynamic Viscosity (kg/ms)
Pure Water (H <sub>2</sub> O)	996	4178	0.615	7.98E-04
Aluminum-Nitride (AlN)	3260	740	285	-

For a single-phase analysis, proper formulation of effective thermal conductivity and viscosity amongst other thermophysical properties are required. The following models are used to compute the effective thermophysical properties for the mass density and specific heat capacity [15], thermal conductivity [16] and Viscosity [17] and the result of the computation for the various concentrations was depicted in Table 3.:

$$\rho_{nf} = (1 - \phi)\rho_{bf} + \phi\rho_p \tag{1}$$

$$Cp_{nf} = \frac{\phi(\rho Cp)_p + (1-\phi)(\rho Cp)_{bf}}{\phi\rho_p + (1-\phi)\rho_{bf}} \tag{2}$$

$$\frac{k_{nf}}{k_{bf}} = \frac{k_p + (n-1)k_{bf} - \phi(n-1)(k_{bf} - k_p)}{k_p + (n-1)k_{bf} + \phi(k_{bf} - k_p)} \tag{3}$$

$$\frac{\mu_{nf}}{\mu_{bf}} = (1 + 2.5\phi + 6.2\phi^2) \tag{4}$$

Where,  $\rho$ ,  $C_p$ ,  $k$ , and  $\phi$  are the density, heat capacity, thermal conductivity, viscosity, and concentration of the nanoparticle, respectively. Whereas the subscripts  $nf$ ,  $p$  and  $bf$  represent singly the nanofluid, nanoparticle and the base fluid.

**Table 3**  
 The result of thermophysical properties of AlN-H<sub>2</sub>O at different volume fractions

Volume fraction	Density (kg/m <sup>3</sup> )	Specific heat (J/kgK)	Thermal conductivity (W/mK)	Viscosity (kg/ms) *10 <sup>-3</sup>	Prandtl No.	$\mu_{nf}/\mu_{bf}$	$k_{nf}/k_{bf}$
0.01	1018.64	4067.97	0.634	0.818	5.25	1.03	1.03
0.03	1063.92	3861.96	0.672	0.862	4.96	1.08	1.09

### 2.3 Boundary Conditions and Governing Equations

The work assumed the nanofluid to be single-phase thereby moving with the same velocity and no-slip between the nanoparticles and the base fluid. Also, it is regarded as Newtonian fluid in a turbulent continuum through the channels made from an Aluminum substrate. The "Velocity inlet" assigned at the inlet and the working fluid enters at a temperature of 303K. The flow is assumed fully developed at the outlet. The "Pressure outlet" imposed at the outlet equals the atmospheric pressure, thus,  $P = 0\text{Pa}$  gauge pressure. A constant heat flux of  $85\text{ W/cm}^2$  is applied on the bottom wall assumed to be in contact with the top of the heat flux dissipating IC, whereas no-slip condition (viscous flow) experienced by all other walls.

Based on the conditions and assumptions mentioned above, we expressed the Navier-Stokes and energy equations in nondimensional forms for continuity, momentum and energy, respectively as follows:

$$\nabla \cdot (\rho_{nf} \cdot \vec{V}) = 0 \quad (5)$$

$$\nabla \cdot (\rho_{nf} \cdot \vec{V} \vec{V}) = \nabla P + \nabla \cdot (\mu_{nf} \cdot \nabla \vec{V}) \quad (6)$$

$$\nabla \cdot (\rho_{nf} \cdot \vec{V} C_p T) = \nabla \cdot (k_{nf} \cdot \nabla T) \quad (7)$$

Where  $\rho_{nf}$  and  $\mu_{nf}$  represent the density and viscosity of the nanofluid, respectively, while  $\vec{V}_m$  is a mass-averaged velocity,  $C_p$ ,  $P$  and  $T$  are Specific heat, Pressure and Temperature, respectively.

Therefore, the non-dimensional parameters used in the equations above are expressed as follows:

$$X = \frac{x}{D_h}; Y = \frac{y}{D_h}; Z = \frac{z}{D_h}; U = \frac{u}{u_{in}}; V = \frac{v}{v_{in}}; W = \frac{w}{w_{in}}; P = \frac{p}{\rho \cdot u_{in}^2} \text{ and } \Theta = \frac{T - T_{in}}{T_w - T_{in}} \quad (8)$$

Further to these governing equations and given chosen turbulent regime for this study, an additional model known as the realizable  $k$ - $\epsilon$  turbulent model was employed. It is presented by Shih *et al.*, [18] based on the pioneering work by Launder and Spalding [19] and its characterized by the turbulent kinetic energy  $k$  and  $\epsilon$  for dissipation of this energy, and respectively expressed as follows:

$$\frac{\partial}{\partial t} (\rho k) + \frac{\partial}{\partial x_j} (\rho k V_j) = \frac{\partial}{\partial x_j} \left[ \left( \mu + \frac{\mu_t}{\sigma_k} \right) \frac{\partial k}{\partial x_j} \right] + G_k + G_b - \rho \epsilon - Y_M + S_k \quad (9)$$

$$\frac{\partial}{\partial t} (\rho \epsilon) + \frac{\partial}{\partial x_j} (\rho \epsilon V_j) = \frac{\partial}{\partial x_j} \left[ \left( \mu + \frac{\mu_t}{\sigma_\epsilon} \right) \frac{\partial \epsilon}{\partial x_j} \right] + \rho C_{1\epsilon} S \epsilon - \rho C_{2\epsilon} \frac{\epsilon^2}{k + \sqrt{\nu \epsilon}} + C_{1\epsilon} \frac{\epsilon}{k} C_{3\epsilon} G_b + S_\epsilon \quad (10)$$

Where  $G_k$  and  $G_b$  represent turbulence kinetic energy generation due to average velocity gradient and buoyancy, respectively.  $Y_m$  is the contribution of the fluctuating dilatation incompressible turbulence to the overall dissipation rate. From Eq. (10), the values of the model constants are:  $C_{1\epsilon}$ ,  $C_{2\epsilon}$ ,  $\sigma_k$  and  $\sigma_\epsilon$  are 1.9, 1.0 & 1.2, respectively.

## 3. Numerical Approach

### 3.1 Solution Strategy

The flow and thermal fields of the fluids in 3-dimensional forced convection are simulated with commercial Computational Fluid Dynamics (CFD) solver ANSYS Fluent v.17.1. The SIMPLE algorithm coupled the velocity and pressure coupling and second-order upwind numerical scheme discretized

the convective transport term of the governing equations. The convergence criterion for the residuals of continuity, momentum, energy, turbulent kinetic and dissipation rates was set to  $10^{-6}$ .

### 3.2 Mesh Independence Check

By varying the element size from 0.08 mm to 0.04 mm with the adaptive method chosen, five different uniform meshes were generated with variable sizes from around 300,000 to around  $3 \times 10^6$ . For all the cases, the meshes are made finer near the wall of the minichannels where the velocity and temperature gradients are anticipated to be large. The simulation was run with water at Re 10,000 for all the cases to ensure independence on the simulation results on the grid sizes and the number of cells generated. Figure 1 shows the close-up of the meshes of the computational domains.

Here only, the result of Case 1 is presented and has relatively similar outcomes with the other cases. The error in the Nusselt numbers and friction factor on the grids with 817,000 and 2,736,000 elements were below 1% as shown in Table 4, thus, to save computing time and memory, the grid with 817000 elements was used for the simulations. Consequence upon these comparisons, the meshes with the same element size of 0.06 mm was chosen for all the cases in this study.

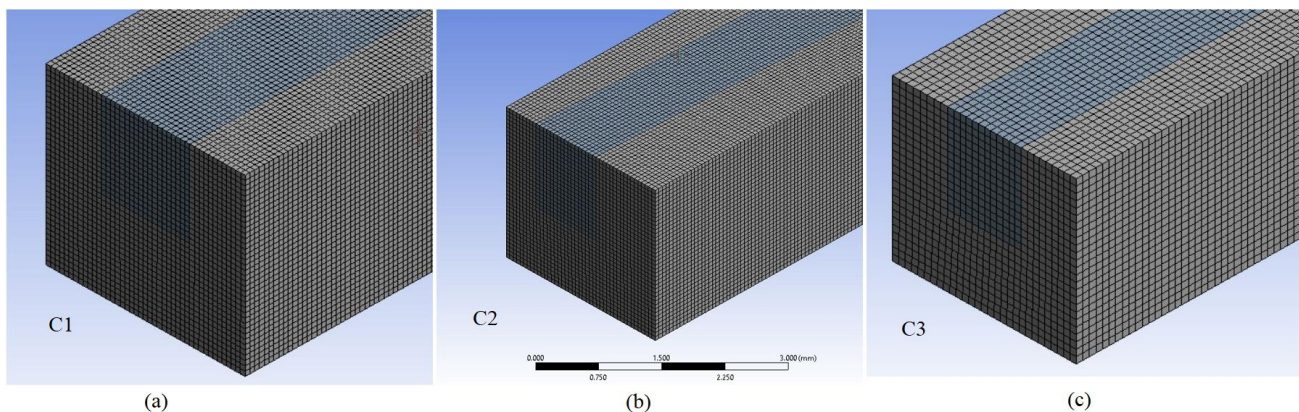


**Fig. 1.** The meshes of the computational domains for (a) Square (b)Wavy and (c) Rectangular

**Table 4**

Values of Pressure drop and Nusselt no for the grids

Mesh/grid	Grid sizes (* $10^6$ )	Pressure drop $\Delta P$	$\Delta P$ error (%)	Nusselt Number	Nu error (%)
M1	0.348	25742.3	0.00	81.4	0.00
M2	0.510	25851.5	0.42	81.4	0.05
<b>M3</b>	<b>0.817</b>	<b>25993.7</b>	<b>0.97</b>	<b>81.2</b>	<b>0.16</b>
M4	1.377	26275.1	2.03	80.9	0.62
M5	2.736	26892.6	4.28	80.4	1.15

### 3.3 Numerical Model Validation

The validation of numerical data was conducted by comparison with established correlations to authenticate the ability of the solver to accurately and reliably predict the outcomes of the simulation as shown in Figure 2. Phillips *et al.*, [20] for the fully developed turbulent region used for local Nusselt number and Filonenko [21] for average friction factor. The maximum deviations of local Nusselt number and average friction factor with the correlation were 9.8% and 15%, respectively. The

deviations are due to variations of testing conditions especially supposition of fully developed flow at the channel inlet, which was unattainable in this study due to the small length of the minichannels.

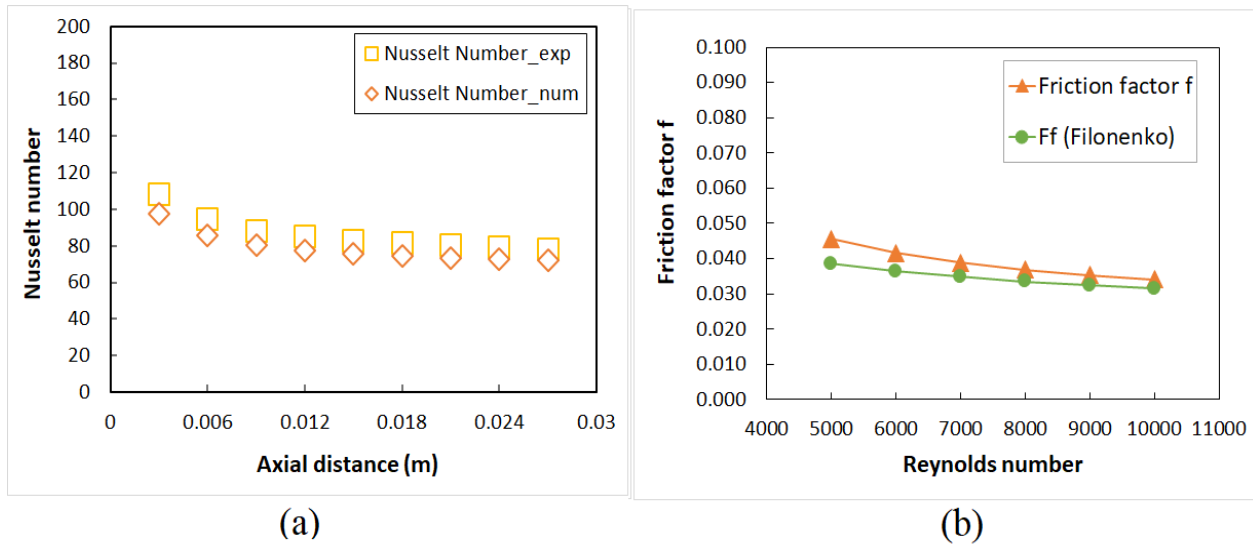


**Fig. 2.** Comparison of experimental and numerical prediction for (a) Local Nusselt number and (b) Average friction factor

#### 4. Results and Discussions

##### 4.1 Heat Transfer Enhancement (HTC)

Figure 3. shows the heat transfer coefficient for the cases at 0.03 volume fraction. It increases with increase in Reynolds number and volume fractions. If  $T_w$ ,  $T_b$  and  $q'_{ch}$  represent the Wall Temperature, the mean fluid temperature and total heat flux, then the local heat transfer coefficient along the minichannel is defined as:

$$h = \frac{q'_{ch}}{T_w - T_b} \quad (11)$$

while the Nusselt number is defined as  $Nu = \frac{hD_h}{k}$  (12)

The interaction of nanoparticles with water molecules by Brownian motion, assist in the enhancement of the effective thermal conductivity of the nanofluid thereby improving convective heat transfer between the fluid and solid interface. The wavy channel (C2) has the highest value while the lowest was found for the square channel (C1). The velocity tends to vary for most of the wavy minichannel which ensures proper mixing unlike the square and rectangular channels which have more uniform velocity profile for most of the channels as shown in Figure 4.

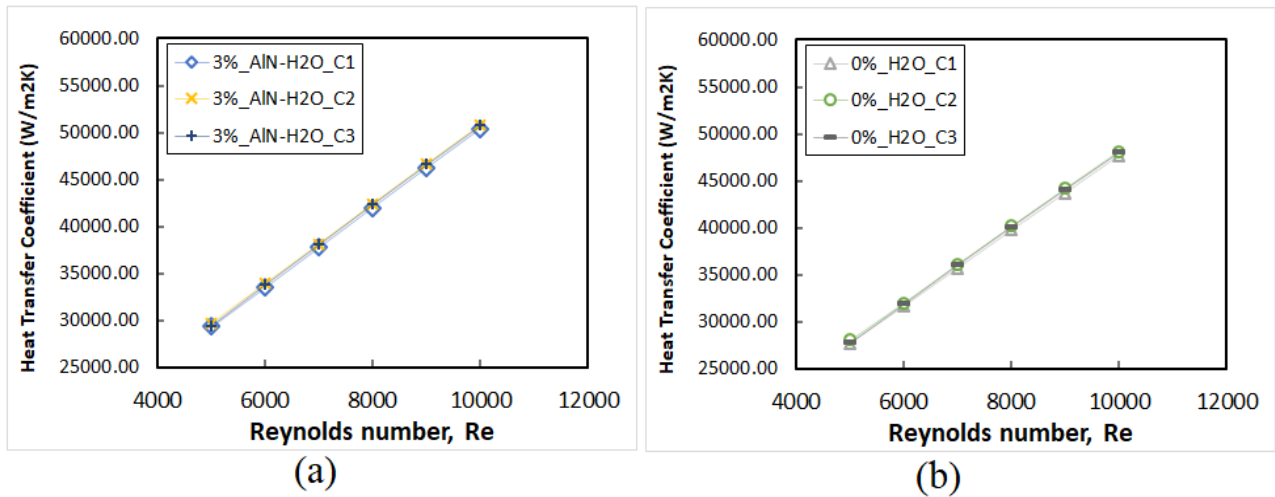


Fig. 3. Variation of HTC with Reynolds number for all cases (a) 0.03 volume fraction & (b) Pure water

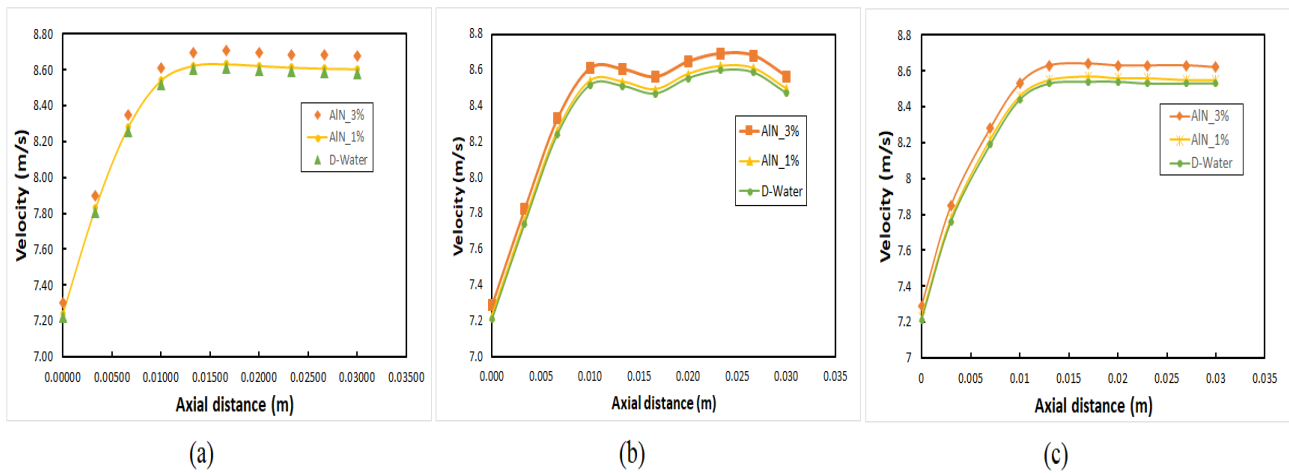


Fig. 4. The velocity profile along the different minichannels (a) Case 1, (b) Case 2 & (c) Case 3

#### 4.2 Effect of Pressure Drop and Friction Factor on Fluids Flow

The effect of pressure drop due to the variation of the Reynolds number for all the cases as shown in Figure 5. The pressure drop can be computed using the following relation:

$$\Delta P = f \left( \frac{L}{D_h} \right) \left( \frac{\rho u_m^2}{2} \right) \quad (13)$$

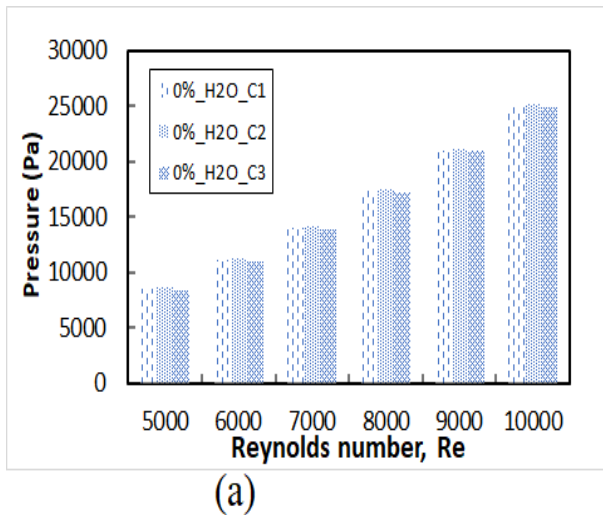
Where  $f$  is the dimensionless friction factor and  $D_h$  is the Hydraulic diameter expressed as:

$$D_h = \frac{4(w \cdot h)}{2(w+h)} \quad (14)$$

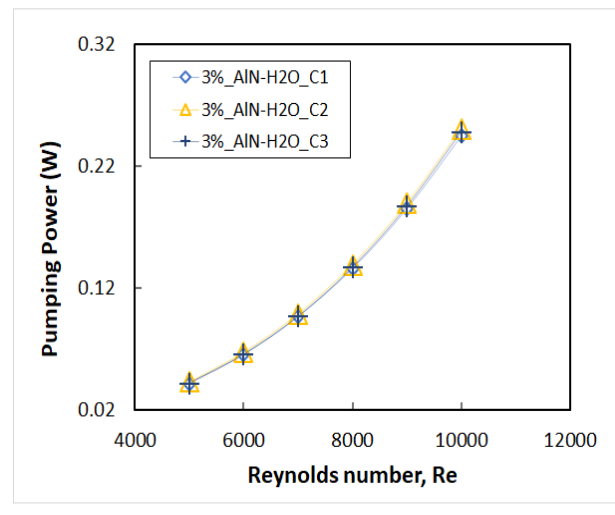
The pressure drops rise linearly with increase in Reynolds for all the cases. This increase can be attributed to the increase in viscosity due to the AIN nanoparticle addition in water, and this effect has more significance on fluid flow than the thickness reduction of the hydrodynamic boundary layer by velocity increment. Though, entrance length was observed to increase with an increase in Reynolds number due to disturbance of boundary layer caused by the convection and the assumptions of slip mechanism. The pressure loss is highest for case 2 due to its lowest surface area compared to other cases. The Pressure drop at Re 10000 when the volume fraction increase from

0.0 and 0.01 to 0.03 rise by about 9% and 6%, respectively. To compensate for the pressure loss, the system requires Pumping power, which is a product of Volume flow rate and Pressure drop denoted as  $\tilde{V}$  and  $\Delta P$ , respectively, and can be computed by the following relation:

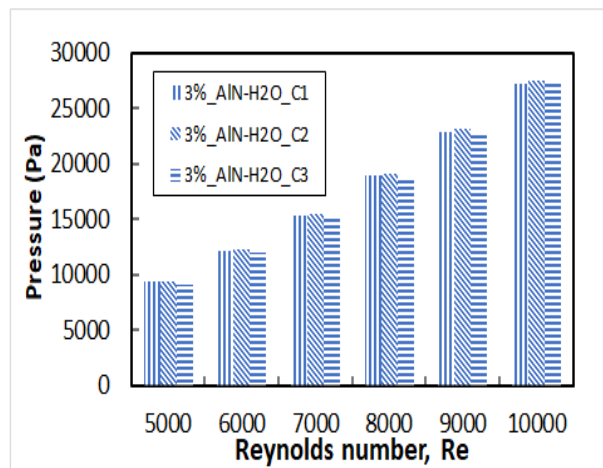
$$PP = \Delta P \cdot \tilde{V} \quad (15)$$



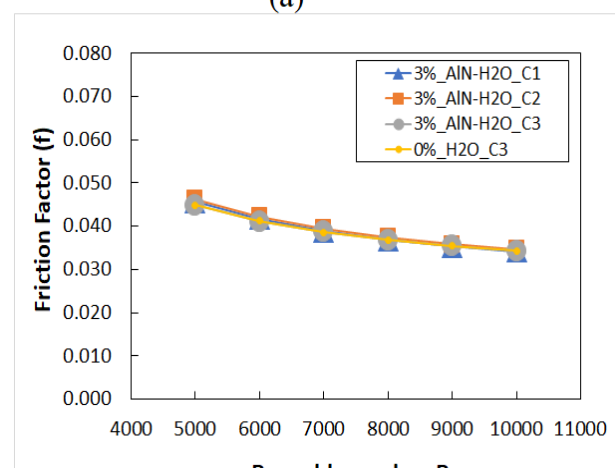
(a)



(a)



(b)



(b)

**Fig. 5.** Pressure drop for all cases at concentrations (a)0% and (b) 3%

**Fig. 6.** Variation with Re for all cases at 0.03vol% (a) Pumping Power and (b) Friction factor

From Figure 6(a), the variation of Pumping Power between the cases are comparatively the same, but slightly higher for Case 2 due to its geometrical constriction at the centre of the cavity. Figure6(b) shows the variation of friction factor with the Reynolds number. The profile of the friction factor is the same for all the volume fractions as well as in pure water. The friction factor tends to decrease as Re increases since the velocity inversely relates to the friction factor. The increase in dynamic viscosity due to increase in nanoparticles loading in the base fluid has a minimal effect on the friction factor. Thus, nanoparticle with small volume fractions can improve heat transfer with minimal friction factor.

### 4.3 Effect of Temperature on the Fluids and the Channel Walls

The temperature increases beyond the thermal entrance length along the minichannels as more heat transferred from the heated wall to the nanofluid as it moves from the inlet to the outlet of the minichannels for all the cases as depicted in Figure 7(a). The increase in effective thermal conductivity and reduction of effective heat capacity of the nanofluid can be attributed to this enhancement. While at the outlet, temperature continuously decreases from around 330K to about 303K. since the expected temperature of enclosed IC is expected not to exceed 353K (80°C), it can be implied that all the geometries can be used for heat sink application, but case 2 with lowest wall temperature with increase Reynolds number indicates that it possesses the higher heat transfer enhancement than the other cases especially with nanofluid as shown in Figure7(b).

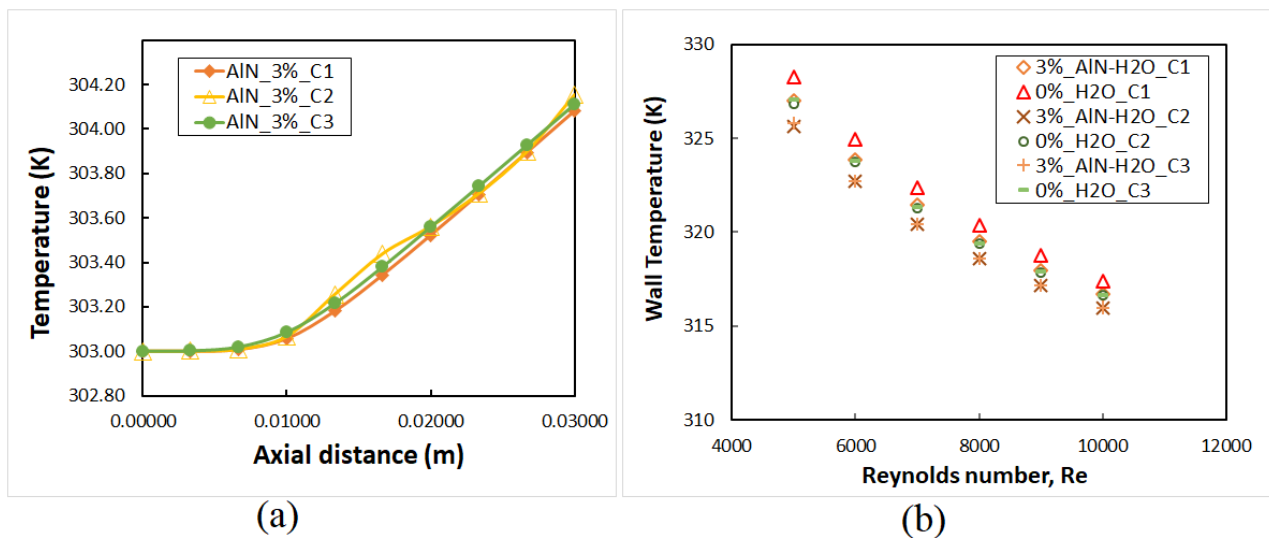


Fig. 7. (a) Temperature profile along the channels (b) Variation of wall Temperature with Re for 0 and 3 vol%

Thermal resistance can be used as an evaluation criterion for the thermal performance of the geometries for heatsink application. Its expressed as follows:

$$R_{th} = \frac{T_{max} - T_{in}}{q_{max} \cdot A_b} \quad (16)$$

Where  $T_{max}$  and  $T_{in}$  represent Maximum Temperature on the wall and Temperature at the inlet.  $q_{max}$  is the maximum heat flux applied and  $A_b$  is the contact area between the heat sink and IC chip interface.

From Figure 8 the thermal resistance is lowest at the highest Re. Also, increasing the volume fraction enhances the convective heat transfer due to Brownian diffusion and eventually reduces the thermal resistance. Among all the cases, the Case 2 has the lowest thermal resistance.

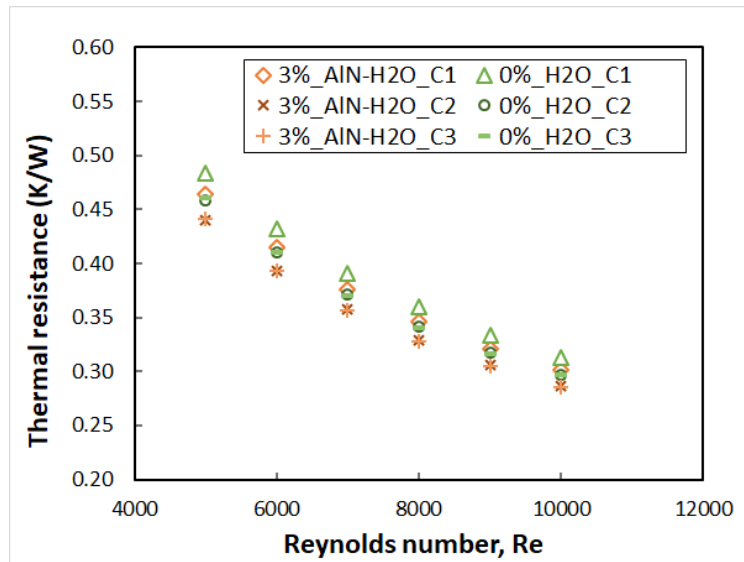


Fig. 8 Effect of Thermal resistance on Reynolds number at 0 and 0.03vol%

## 5. Conclusions

In this study, we investigated numerically the heat transfer and flow of Aluminum-Nitride-Water Nanofluid flowing inside three different mini-sized geometries having an identical hydraulic diameter. The effects of nanoparticles volume fractions and variation of geometry were analysed numerically. The important observations are:

- i. There is convective heat transfer enhancement between the fluid and solid interface due to molecular interaction of nanoparticles with water molecules as observed in the Brownian diffusion phenomenon which augments the effective thermal conductivity of the nanofluid. The enhancement is more noticeable for the wavy channel (C2) and least for the square channel (C1).
- ii. Case 2 indicated the highest pressure loss due to its lowest surface area compared to other cases. The Pressure drop at Re 10000 when the volume fraction increase from 0.01 to 0.03 rise by about 6%.
- iii. The variation of friction factor with flow velocity in terms of Re is similar for all the volume fractions as well as in pure water. The increase in dynamic viscosity due to increase nanoparticles loading in the base fluid affects friction factor minimally. Hence, nanofluid with small volume fractions can augment heat transfer with minimal friction factor.
- iv. The minichannel outlet temperature depreciates from around 330K to about 303K. Since the expected temperature of enclosed IC is expected not to exceed 353K (80°C), it can be implied that all the geometries can be used for heat sink application, but case 2 with lowest wall temperature with increase Reynolds number indicates that it possesses the higher heat transfer enhancement than the other cases, especially with nanofluid.
- v. Based, on the hydrothermal performance of the wavy minichannel geometry i.e. case 2, it can be regarded as the best candidate among the cases for minichannel heatsink application.

## Acknowledgement

The researchers would like to thank Universiti Teknologi Malaysia and the Ministry of Education, Malaysia for supporting this research activity. This research was funded by an International grant from the Takasago Thermal Engineering Co. Ltd. (Grant no.: R.K130000.7343.4B472).

## References

- [1] Choi, Stephen US, and Jeffrey A. Eastman. *Enhancing thermal conductivity of fluids with nanoparticles*. No. ANL/MSD/CP-84938; CONF-951135-29. Argonne National Lab., IL (United States), 1995.
- [2] Hashim, Ishak, A. I. Alsabery, Mikhail A. Sheremet, and A. J. Chamkha. "Numerical investigation of natural convection of Al<sub>2</sub>O<sub>3</sub>-water nanofluid in a wavy cavity with conductive inner block using Buongiorno's two-phase model." *Advanced Powder Technology* 30, no. 2 (2019): 399-414.  
<https://doi.org/10.1016/j.appt.2018.11.017>
- [3] Ajeel, Raheem K., WS-IW Salim, and Khalid Hasnan. "An experimental investigation of thermal-hydraulic performance of silica nanofluid in corrugated channels." *Advanced Powder Technology* 30, no. 10 (2019): 2262-2275.  
<https://doi.org/10.1016/j.appt.2019.07.006>
- [4] Kumar, Vivek, and Jahar Sarkar. "Numerical and experimental investigations on heat transfer and pressure drop characteristics of Al<sub>2</sub>O<sub>3</sub>-TiO<sub>2</sub> hybrid nanofluid in minichannel heat sink with different mixture ratio." *Powder technology* 345 (2019): 717-727.  
<https://doi.org/10.1016/j.powtec.2019.01.061>
- [5] Liu, Donglin, Yuanxiang Zhou, Ying Yang, Ling Zhang, and Fubao Jin. "Characterization of high performance AlN nanoparticle-based transformer oil nanofluids." *IEEE Transactions on Dielectrics and Electrical Insulation* 23, no. 5 (2016): 2757-2767.  
<https://doi.org/10.1109/TDEI.2016.7736835>
- [6] Wozniak, Maciej, Anna Danelska, Pawel Rutkowski, and Dariusz Kata. "Thermal conductivity of highly loaded aluminium nitride-poly (propylene glycol) dispersions." *International Journal of Heat and Mass Transfer* 65 (2013): 592-598.  
<https://doi.org/10.1016/j.ijheatmasstransfer.2013.06.048>
- [7] Wanic, Michał, David Cabaleiro, Samah Hamze, Jacek Fal, Patrice Estellé, and Gawel Żyła. "Surface tension of ethylene glycol-based nanofluids containing various types of nitrides." *Journal of Thermal Analysis and Calorimetry* 139, no. 2 (2020): 799-806.  
<https://doi.org/10.1007/s10973-019-08512-1>
- [8] Baker, Colin C., Abdullah Ceylan, and S. Ismat Shah. "Reactive gas condensation synthesis of aluminum nitride nanoparticles." *Journal of nanoscience and nanotechnology* 6, no. 1 (2006): 146-150.  
<https://doi.org/10.1166/jnn.2006.17920>
- [9] Dongliang, Zhao, and Gao Ling. "Study on the preparation of aluminum nitride with high thermal conductivity." In *2014 15th International Conference on Electronic Packaging Technology*, pp. 493-495. IEEE, 2014.  
<https://doi.org/10.1109/ICEPT.2014.6922703>
- [10] Taha-Tijerina, Jaime, Natalia Cadena-De La Peña, Rodrigo Cue-Sampedro, and Carlos Rivera-Solorio. "Thermophysical evaluation of dielectric mineral oil-based nitride and oxide nanofluids for thermal transport applications." *Journal of Thermal Science and Technology* 14, no. 1 (2019): JTST0007-JTST0007.  
<https://doi.org/10.1299/jtst.2019jtst0007>
- [11] Yu, Wei, Huaqing Xie, Yang Li, and Lifei Chen. "Experimental investigation on thermal conductivity and viscosity of aluminum nitride nanofluid." *Particuology* 9, no. 2 (2011): 187-191.  
<https://doi.org/10.1016/j.partic.2010.05.014>
- [12] Żyła, Gawel, and Jacek Fal. "Experimental studies on viscosity, thermal and electrical conductivity of aluminum nitride-ethylene glycol (AlN-EG) nanofluids." *Thermochimica acta* 637 (2016): 11-16.  
<https://doi.org/10.1016/j.tca.2016.05.006>
- [13] Wozniak, Maciej, Anna Danelska, Dariusz Kata, and Mikolaj Szafran. "New anhydrous aluminum nitride dispersions as potential heat-transferring media." *Powder technology* 235 (2013): 717-722.  
<https://doi.org/10.1016/j.powtec.2012.11.023>
- [14] Sarkar, Jahar. "A critical review on convective heat transfer correlations of nanofluids." *Renewable and sustainable energy reviews* 15, no. 6 (2011): 3271-3277.  
<https://doi.org/10.1016/j.rser.2011.04.025>

- [15] Xuan, Yimin, and Wilfried Roetzel. "Conceptions for heat transfer correlation of nanofluids." *International Journal of heat and Mass transfer* 43, no. 19 (2000): 3701-3707.  
[https://doi.org/10.1016/S0017-9310\(99\)00369-5](https://doi.org/10.1016/S0017-9310(99)00369-5)
- [16] Hamilton, R. L<sup>III</sup>, and O. K. Crosser. "Thermal conductivity of heterogeneous two-component systems." *Industrial & Engineering chemistry fundamentals* 1, no. 3 (1962): 187-191.  
<https://doi.org/10.1021/i160003a005>
- [17] Batchelor, G. K. "The effect of Brownian motion on the bulk stress in a suspension of spherical particles." *Journal of fluid mechanics* 83, no. 1 (1977): 97-117.  
<https://doi.org/10.1017/S0022112077001062>
- [18] T.-H. Shih, W. W. Liou, A. Shabbir, Z. Yang, and J. Zhu, "A new k- $\epsilon$  eddy viscosity model for high Reynolds number turbulent flows," *Comput. Fluids*, vol. 24, no. 3, pp. 227–238, 1995.  
[https://doi.org/10.1016/0045-7930\(94\)00032-T](https://doi.org/10.1016/0045-7930(94)00032-T)
- [19] B. E. Launder and D. B. Spalding, "The numerical computation of turbulent flows," *Comput. Methods Appl. Mech. Eng.*, vol. 3, no. 2, pp. 269–289, 1974.  
[https://doi.org/10.1016/0045-7825\(74\)90029-2](https://doi.org/10.1016/0045-7825(74)90029-2)
- [20] Phillips, Richard J. "Microchannel heat sinks." *The Lincoln Laboratory Journal* 1, no. 1 (1988): 31-48.
- [21] Minea, Alina Adriana. "Numerical studies on heat transfer enhancement and synergy analysis on few metal oxide water based nanofluids." *International Journal of Heat and Mass Transfer* 89 (2015): 1207-1215.  
<https://doi.org/10.1016/j.ijheatmasstransfer.2015.06.039>